Physics Letters B 798 (2019) 134954

Contents lists available at ScienceDirect

Physics Letters B

www.elsevier.com/locate/physletb

Insights into the dynamics of breakup of the halo nucleus ^{11}Be on a ^{64}Zn target

A. Di Pietro [a], A.M. Moro [b,*], Jin Lei [b,1,*], R. de Diego [b,2]

[a] INFN-Laboratori Nazionali del Sud and Sezione di Catania, Via S. Sofia 62, I-95123 Catania, Italy
[b] Departamento de Física Atómica, Molecular y Nuclear, Facultad de Física, Universidad de Sevilla, Apartado 1065, E-41080 Sevilla, Spain

ARTICLE INFO

Article history:
Received 27 June 2019
Received in revised form 12 September 2019
Accepted 17 September 2019
Available online 20 September 2019
Editor: J.-P. Blaizot

Keywords:
^{11}Be
Reactions with halo nuclei
Breakup

ABSTRACT

We reexamine the elastic and breakup observables of the ^{11}Be + ^{64}Zn reaction at the near-barrier energy of 28.7 MeV. The measured quasi-elastic data are compared with CDCC and extended CDCC (XCDCC) calculations, the latter including the effect of the ^{10}Be deformation.
The angular distribution of emitted ^{10}Be fragments, reported in the original analysis of this experiment, along with newly extracted ^{10}Be energy distributions, are compared with calculations for the elastic breakup and non-elastic breakup contributions. Elastic breakup, computed with CDCC, accounts for most of the observed yields. The remaining difference (∼20%) is attributed to non-elastic breakup events (neutron absorption or target excitation) as confirmed by calculations performed with the model of Ichimura, Austern and Vincent (1985) [14].
Finally, the effect of post-acceleration in the energy distribution is investigated. This effect is well accounted for by the present CDCC calculations and, according to simple kinematical considerations, is estimated to be of the order of 1 MeV, and roughly independent of the scattering angle.

1. Introduction

The discovery of exotic atomic nuclei in the proximity of the proton and neutron drip lines constitutes one of the major milestones in nowadays nuclear physics. Often, these nuclei exhibit novel and striking phenomena not found in the case of stable nuclei. For example, for some light drip-line nuclei, valence nucleons travel beyond the surface of the central *core*, forming an extended cloud known as nuclear *halo*. Much of our present knowledge of the structure of these exotic systems stems from the analysis of nuclear collisions of these nuclei with a stable nucleus. Due to the weak binding, one may anticipate that breakup will be a major reaction channel, as it is indeed confirmed experimentally. Furthermore, one may also expect some decoupling of the single-particle motion of the halo with respect to the remaining system (*core*). This has motivated the application of few-body reactions models, such as the Continuum–Discretized Coupled–Channels (CDCC) method [1], semiclassical approaches [2–5] and, more recently, also the Faddeev equations [6].

Despite the usefulness of these methods, the strict few-body picture of the reaction implies a drastic simplification of the many-body scattering problem. Comparisons of experimental observables, such as elastic, inelastic and breakup differential cross sections, with the predictions of these formalisms allows establishing the limits of validity of the few-body description of the structure and dynamics of these nuclei and serve to extract valuable information on their structure. Deviations from experimental data evidence limitations of the structure description, the reaction dynamics or the effective interactions.

Among these deviations from the strict few-body picture, two of them have recently received particular attention, namely, (i) the so-called core excitations (CEX) and (ii) the presence of non-elastic breakup (NEB) contributions in the inclusive breakup observables. The CEX refer to possible excitations of the projectile fragments which, in the case of halo nuclei, correspond to excitations of the *core* subsystem. These CEX modify, on one hand, the structure of the projectile, by introducing core-excited admixtures in the projectile states and, on the other hand, leads to excitations and de-excitations of the core during the reaction. To account for CEX, an extended version of the CDCC method (coined XCDCC) has been

* Corresponding authors.
E-mail address: moro@us.es (A.M. Moro).
[1] Current address: Institute of Nuclear and Particle Physics, and Department of Physics and Astronomy, Ohio University, Athens, Ohio 45701, USA.
[2] Current address: Departamento de Estructura de la Materia, Física Térmica y Electrónica, Universidad Complutense de Madrid, E-28040 Madrid, Spain.

https://doi.org/10.1016/j.physletb.2019.134954

developed [7] and applied to several reactions induced by ^{11}Be [8, 9] and ^{19}C [10].

Regarding the NEB, it corresponds to projectile breakup accompanied by target excitation or by capture of one of the projectile constituents by the target. These contributions are not accounted for by the CDCC or XCDCC methods, which provide only the so-called *elastic breakup* (EBU) part. Because of the large number of accessible states, explicit inclusion of all channels contributing to NEB is not feasible in practice. The evaluation of non-elastic cross sections can be more efficiently done making use of inclusive breakup models. These were proposed in the 1980s [11–15] but they have not been fully tested and applied until recently [16–18]. In particular, these models have never been applied to the case of halo nuclei.

In this work, we investigate the influence of CEX and NEB in the reaction of ^{11}Be on a ^{64}Zn target, measured at ISOLDE by Di Pietro et al. [19]. The quasielastic (i.e. elastic+inelastic) and breakup data from this experiment have been subject of many studies, including optical model [19], CDCC [20–22] and semiclassical calculations [23,24]. In [20], the quasi-elastic data could be well reproduced by standard CDCC calculations, but the inclusive breakup data (^{10}Be angular distribution) was significantly underestimated. In a later work, the same data were compared with XCDCC calculations [8]. Although these calculations predicted larger breakup cross sections, improving the agreement with the data, some underestimation remained.

In this Letter we present new calculations for the elastic and inclusive breakup data of this reaction. We report also on new experimental results of the same experiment not published before, corresponding to the energy spectra of the ^{10}Be fragments. These data are compared with CDCC and XCDCC calculations, using an augmented modelspace with respect to previous studies. In addition, the contribution of NEB in the inclusive ^{10}Be data, using the inclusive breakup model of Ichimura, Austern and Vincent (IAV), is also explored. Finally, the phenomenon of post-acceleration is investigated using a simple model.

The paper is organized as follows. In Section 2, we briefly discuss the experimental analysis of the new data. Then, in Sec. 3, we outline the theoretical frameworks used, namely, the XCDCC method and the IAV model. The calculations performed with these models are compared in Section 4 with the quasielastic and inclusive breakup data of Ref. [19], along with new data extracted from the same reaction, corresponding to the energy distributions of ^{10}Be fragments. Finally, in Sec. 5 the main conclusions of this work are summarized.

2. Experimental analysis

The ^{11}Be + ^{64}Zn reaction was measured at the REX-ISOLDE facility. Details of the experimental set-up have been reported in Refs. [19] and [20]. The ^{10}Be fragments produced in the reaction were detected and identified, in charge and mass, in the angular range $15^\circ \leq \theta_{\rm lab} \leq 42^\circ$. In Fig. 1 it is shown a 2D-spectrum of ΔE *vs.* the total energy ($E_{\rm tot}$). The latter was reconstructed by considering, in addition to the energy deposited in the two stages of detection (ΔE and $E_{\rm res}$), the energy loss of the beam and emitted particles in the target, and the energy loss of the particles in the detector dead layers. The energy loss correction was done on an event-by-event basis. In the spectrum shown in this figure it was assumed, for the energy loss calculations, that the emitted fragment was ^{10}Be. Therefore, the energy information is correct for ^{10}Be events but not for ^{11}Be ones.

As can be seen from the figure, there is a band of events, starting from the elastic scattering locus, for which the ΔE energy decreases for decreasing total energy. These events are elastic scattering events for which the total energy is not correctly measured due to incomplete charge collection in the ΔE detector most probably due to interstrip effects [25,26]. Although interstrip events producing signals above threshold into two neighbour strips have been excluded from the data analysis, some of them might still remain [26]. These are background events and must be removed from the energy spectra. To do that, the same gate used for selecting ^{10}Be events, shown in black in Fig. 1, was shifted so as to include a similar fraction of background events as in the ^{10}Be gate (red gate); the energy shift varied depending upon angle and the same was for the fraction of background events, since it depended on the elastic scattering rate on the detector. To obtain background-subtracted energy distribution of ^{10}Be, the spectrum corresponding to the background gate had to be shifted, before subtraction, by the same $E_{\rm tot}$ as the one used to produce the red gate.

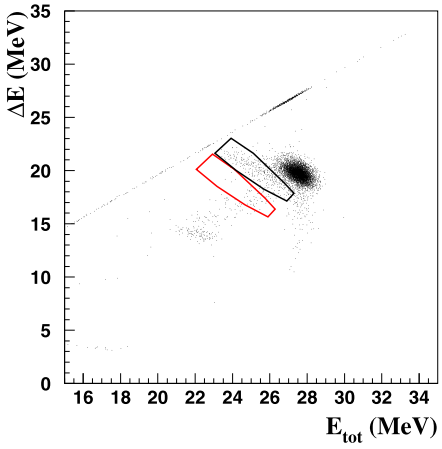

Fig. 1. ΔE *vs.* $E_{\rm tot}$ bidimensional spectrum at $\theta_{\rm lab} = 20^\circ$. The polygons shown in black and red enclose, respectively, ^{10}Be events and background events (see text for details).

3. Theoretical framework

For the interpretation of the present data we employ state-of-the-art methods for the computation of breakup cross sections. For the EBU cross sections, we use the recently developed XCDCC method [7,8], a generalization of the standard CDCC formalism that takes into account the effect of the deformation of the core subsystem in the projectile and also its possible excitations and de-excitations during the collision. In particular, we treat the n-^{10}Be system using a particle-plus-rotor model (PRM) with the Hamiltonian of Ref. [27]. This Hamiltonian consists of central and spin-orbit parts, with the usual Woods-Saxon volume and derivative shapes, respectively. To account for the coupling with the 2^+ state of the core, the central potential is deformed using a deformation parameter $\beta_2 = 0.67$ [28] and later expanded in multipoles. The quadrupole terms are responsible for the coupling between the ^{10}Be g.s. and the 2^+ excited state, giving rise to core-excited admixtures in the ^{11}Be states. The resultant ground-state wave function has a 85% of $s_{1/2}$, consistent with recent *ab-initio* calculations based on the no-core-shell-model (NCSM) formalism [29].

The ^{11}Be continuum was discretized using a *binning* procedure. As a consequence of the ^{10}Be deformation, these continuum states contain also admixtures of core-excited components [7]. Continuum states up to maximum orbital angular momentum $\ell_{\rm max} = 9$, total angular momentum $J^\pi_p = 1/2^\pm, 3/2^\pm, \ldots, 17/2^\pm$ and maximum excitation energy ranging from 8 to 12 MeV (depending on J^π_p) were considered in the calculations. The ^{10}Be + ^{64}Zn and

$n + {}^{64}$Zn potentials were taken from Refs. [19] and [30], respectively. For comparison purposes, we have performed also conventional CDCC calculations, using the single-particle neutron-core potential of Ref. [5]. For consistency, these calculations use the same ^{10}Be + ^{64}Zn and n-^{64}Zn interactions as in the XCDCC calculations. Continuum states were discretized using the standard binning procedure, including partial waves up to $\ell_{\max} = 9$.

To evaluate the non-elastic breakup contributions we make use of the Ichimura, Austern, Vincent (IAV) model [14], which has been recently reexamined and implemented by several groups [16–18]. The IAV model for NEB is based on a participant-spectator picture, which can be schematically represented as $a + A \to b + B^*$, where the projectile a dissociates into $b + x$, but only the fragment b (the spectator particle) is detected. The participant particle x corresponds to the unobserved particle (the neutron in our case). The residual nucleus B^* denotes any possible final state of the $x + A$ system. When x survives after the reaction and A remains in its ground state, we have EBU which, in this work, is calculated with XCDCC. To account for all possible non-elastic processes of the participant with the target nucleus, the IAV model makes use of the Feshbach projection formalism and closure of the neutron-target final states. The resultant NEB double differential cross section with respect to the angle and energy of the core fragment, is given by

$$\left.\frac{d^2\sigma}{dE_b d\Omega_b}\right|_{\rm NEB}^{\rm IAV} = -\frac{2}{\hbar v_i}\rho_b(E_b)\langle\psi_x(\vec{k}_b)|W_{xA}|\psi_x(\vec{k}_b)\rangle, \qquad (1)$$

where iW_{xA} is the imaginary part of the $x - A$ optical potential U_{xA}, $\rho_b(E_b)$ the density of states of the b particle, and $\psi_x(\vec{k}_b, \vec{r}_x)$ is the so-called x-channel wavefunction, which describes the $x - A$ relative motion when the target is in the ground state and the b particle scatters with momentum $\vec{k}_b$. This x-channel wavefunction is obtained from the solution of the inhomogeneous equation

$$(E_x - K_x - U_{xA})\psi_x(\vec{k}_b, \vec{r}_x) = \langle\vec{r}_x\chi_b^{(-)}(\vec{k}_b)|V_{\rm post}|\chi_a^{(+)}\phi_a\rangle, \qquad (2)$$

where $E_x = E - E_b$, $V_{\rm post} \equiv V_{bx} + U_{bA} - U_{bB}$ and $\chi_b^{(-)}(\vec{k}_b)$ is a distorted wave describing the relative motion of the outgoing ^{10}Be fragment and the $A + x$ system.

In the present calculations, the projectile wave function, $\phi_a(\vec{r}_{bx})$ was generated with the same ^{11}Be model used in the CDCC calculations [5] whereas the entrance and exit channel distorted waves ($\chi_a^{(+)}$ and $\chi_b^{(-)}$) were calculated with the optical model potentials derived in [19] from the fit of the ^{11}Be quasi-elastic scattering data and the ^{11}Be elastic scattering data, respectively.

4. Comparison with data

In this section we compare the calculations with the data from Ref. [19], and also with the newly extracted data for the inclusive ^{10}Be distributions.

We first consider the quasielastic cross section displayed in the upper panel of Fig. 2. The CDCC and XCDCC calculations are found to yield almost identical results and reproduce very well the data in the full angular range. However, the separate elastic and inelastic cross sections predicted by these calculations are rather different, as shown in the bottom panel of this figure. The angle-integrated inelastic cross sections are 940 and 437 mb for the CDCC and XCDCC calculations, respectively. This effect was also found in Ref. [31], where the ^{11}Be + ^{197}Au data was analysed with the CDCC and XCDCC methods. In that case, both observables could be separated experimentally and were found to be very well reproduced by XCDCC, whereas the CDCC calculation could not reproduce any of them satisfactorily. The difference was attributed to the reduced $B(E1)$ strength predicted by the deformed ^{11}Be model, in better agreement with Coulomb dissociation experiments and lifetime measurements [32]. A similar effect seems to be taking place in the present reaction, but new data for the separate elastic and inelastic cross sections would be of interest to confirm it. We note that the link between the inelastic cross section for this reaction and the underlying $B(E1)$ value was studied in detail in Ref. [22], where it was shown that, below the grazing angle, the full CDCC calculation is very well reproduced by a first order pure E1 calculation.

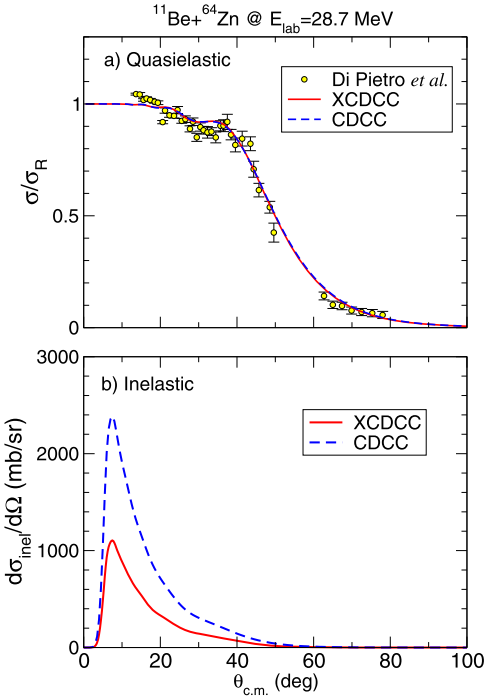

Fig. 2. (a) Experimental [19] and calculated quasielastic differential cross section, as a function of the ^{11}Be CM angle, for the reaction ^{11}Be+^{64}Zn at 28.7 MeV. (b) Inelastic differential cross section for the excitation of the ^{11}Be($1/2^-$) excited state, computed with the CDCC and XCDCC methods.

We consider now the inclusive breakup cross sections, consisting on angular and energy distributions of ^{10}Be singles. We notice that, for the CDCC and XCDCC results, the breakup cross sections are more naturally expressed in terms of the scattering angle of the c.m. of the outgoing $n + {}^{10}$Be pair. To obtain the ^{10}Be angular and energy distributions, one needs to calculate the triple-differential cross sections by applying the appropriate kinematical transformation to the scattering amplitudes computed with CDCC/XCDCC. In the CDCC case, this was done by using the formalism presented in Ref. [33], whereas for the XCDCC case a recently proposed extension of this formalism was used [9].

The computed ^{10}Be angular distributions are compared with the data in Fig. 3. It can be seen that CDCC and XCDCC give almost identical results, confirming the results of [9] performed in a smaller modelspace ($\ell_{\max} = 5$). However, this EBU contribution alone underestimates the magnitude of the data by about 20%. This underestimation suggests that other, non-elastic breakup (NEB), mechanisms contribute also to the inclusive ^{10}Be cross sections.

We have computed these NEB contribution with the IAV model [cf. Eq. (1)], which is shown with the dot-dashed line in Fig. 3. It exhibits a bell-shaped form, with a maximum around 35°. This contribution is rather significant for angles larger than 10°. The total inclusive breakup, given by the sum of the EBU and NEB contributions, give a good overall account of the experimental data,

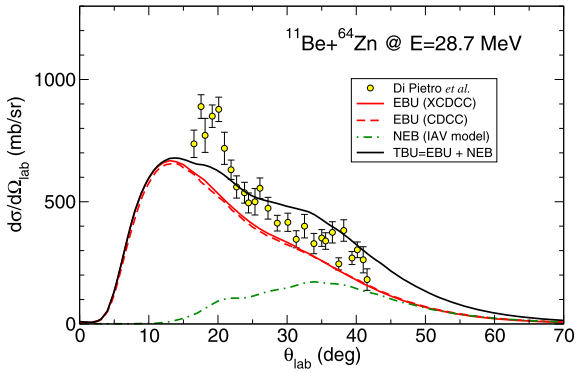

Fig. 3. Experimental and calculated differential breakup cross section, as a function of the ^{10}Be laboratory scattering angle, for the reaction ^{11}Be+^{64}Zn at 28.7 MeV. The elastic breakup contributions (from CDCC and XCDCC calculations) and the nonelastic breakup contribution (IAV model) are compared with the data from Ref. [20].

with some remaining underprediction at the smaller angles, and some overestimation for $\theta = 30^\circ - 40^\circ$.

Further insight into the reaction dynamics can be obtained from the ^{10}Be energy distributions. This is shown in Fig. 4 for some selected angles of ^{10}Be. The experimental distributions display an asymmetric shape, with a tail extending to low energies. For ^{10}Be energies above the peak, all the distributions exhibit an apparent drop showing a kinematical cutoff derived from the energy conservation as well as the interplay between the phase space factor and the breakup amplitude in the semi-inclusive cross sections. For the calculations we show only the results from CDCC, since those obtained with XCDCC are very similar. At the two smaller scattering angles (15.5° and 18°) the calculated inclusive breakup is dominated by the EBU part, and reproduces reasonably well the data. At larger angles (see panels (c) and (d)) the NEB becomes important, and its inclusion is essential to explain the data.

It is noticeable that the experimental distributions peak at an energy which is larger than the simple estimate given by 10/11 times the energy of the outgoing ^{11}Be* system, assuming a binary reaction with a Q-value equal to minus the excitation energy of this system. This simple estimate is indicated by the orange arrows in Fig. 4 which, as can be seen, underpredict the energy of the maximum by about 1 MeV. This *post-acceleration* of the ^{10}Be fragments can be understood as follows. When the projectile approaches the target, part of its kinetic energy will be converted into Coulomb potential energy. For a binary process, such as elastic or inelastic scattering, this potential energy will be transformed again into kinetic energy when the ejectile flies away. However, for a breakup process, the projectile will eventually dissociate into $^{10}\mathrm{Be} + n$ during the collision. After this point, the Coulomb energy will be converted into kinetic energy of the charged fragment, ^{10}Be. Denoting the breakup distance by R_{bu} the additional kinetic energy gained by the ^{10}Be core with respect to the binary process turns out to be

$$\Delta E = \frac{m_n}{m_n + m_c} \frac{Z_c Z_t e^2}{R_{\mathrm{bu}}}, \tag{3}$$

where $Z_{c,t}$ are the core and target charges and $m_{n,c}$ the neutron and core masses.

We have evaluated this formula, assuming for the breakup radius the distance of closest approach in a classical Coulomb trajectory. When this energy shift is added to $(10/11)E(^{11}\mathrm{Be}^*)$, one gets the green arrow shown in Fig. 4 which, as can be seen, agrees very well with the observed experimental centroids.

We have repeated these calculations for other angles and the results are shown in Fig. 5, where we plot the final energy of the ^{10}Be fragments as a function of the scattering angle. The orange line corresponds to the simple estimate $(10/11)E(^{11}\mathrm{Be}^*)$, whereas the green solid line is the result of adding the post-acceleration ΔE effect according to the simple estimate (3). For the data, we have considered the maximum of the energy distribution at the corresponding scattering angle. It is seen that the calculations including post-acceleration reproduce perfectly well these data. Moreover, it can be seen that the energy shift becomes larger as the scattering angle increases, due to the fact that the breakup radius decreases for larger scattering angles. These results indicate that this breakup reaction is not a simple one-step mechanism, but involves additional, higher-order effects which are well accounted for by the simple kinematical estimates as well as by the more sophisticated CDCC calculations.

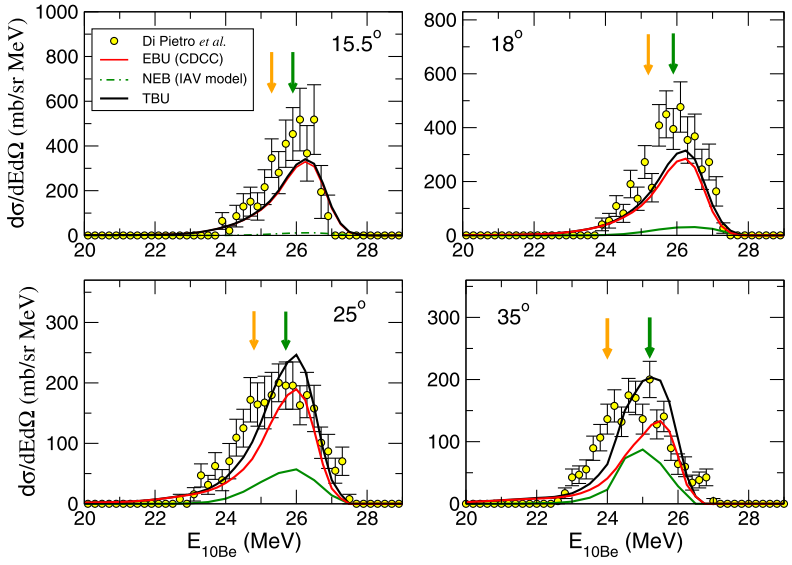

Fig. 4. Experimental and calculated breakup double differential cross-section, as a function of the ^{10}Be laboratory energy, for selected values of the scattering angle. The orange and green arrows correspond to the estimated ^{10}Be energies excluding and including post-acceleration, respectively (see text for details).

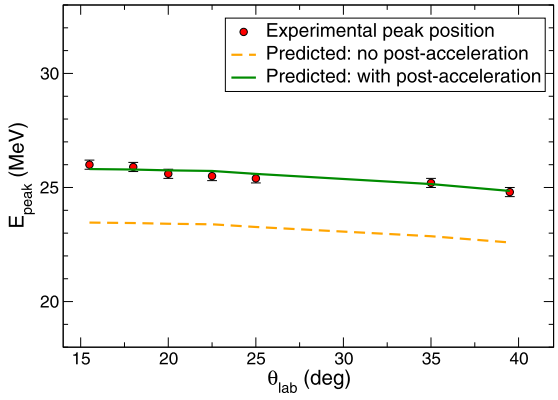

Fig. 5. Experimental position of the centroid of the ^{10}Be energy distribution as a function of the laboratory angle. The dashed orange and solid green lines correspond to the predicted outgoing ^{10}Be energy without and with post-acceleration effect, respectively (see text for details).

5. Conclusions

To summarize, we have investigated the dynamics of the elastic and breakup of the halo nucleus ^{11}Be on a ^{64}Zn target, with emphasis in those effects which go beyond the strict few-body picture of the reaction, namely, core excitations and non-elastic breakup. Quasielastic and inclusive breakup data (^{10}Be singles) have been compared with state-of-the-art reaction calculations. The quasielastic data are equally well reproduced by CDCC and extended CDCC (XCDCC) calculations, with the latter including effects arising from ^{10}Be deformation. Both methods predict however very different inelastic cross sections for the population of the ^{11}Be bound excited state. Therefore, ^{10}Be deformation has a sizable effect on the inelastic scattering cross section, but a very small effect on the quasielastic and breakup cross sections. This contrasts with the case of the proton target, for which a significant enhancement of the breakup cross section was found due to dynamical core excitation effects [8,34,35].

The CDCC and XCDCC calculations predict also similar elastic breakup cross sections, but they underestimate the magnitude of the data by about ∼20%. This underestimation is attributed to the presence of non-elastic breakup contributions. Inclusion of this contribution, using the model of Ichimura, Austern and Vincent, is found to reproduce rather well the experimental angular and energy distributions of the ^{10}Be fragments.

We have also analysed the post-acceleration effect observed in the energy distribution of the ^{10}Be fragments. This effect can be explained assuming that the breakup takes place in the proximity of the target, around the distance of closest approach, and that the Coulomb energy originally carried by the ^{11}Be projectile is finally transferred to the ^{10}Be core. A quantitative estimate of this effect, using as the breakup radius the distance of closest approach for a classical Coulomb trajectory, explains very well the experimental position of the energy distribution peak.

Acknowledgements

We are grateful to R. Morillon for providing us the $n + {}^{64}$Zn potential parameters in a convenient tabular form. This project has received funding from the Spanish Government under project No. FIS2014-53448-C2-1-P and FIS2017-88410-P and by the European Union's Horizon 2020 research and innovation program under grant agreement No. 654002. One of us (R.D.) acknowledges support by a postdoctoral fellowship from the Complutense University of Madrid.

References

[1] N. Austern, Y. Iseri, M. Kamimura, M. Kawai, G. Rawitscher, M. Yahiro, Phys. Rep. 154 (1987) 125, https://doi.org/10.1016/0370-1573(87)90094-9.
[2] S. Typel, G. Baur, Phys. Rev. C 50 (1994) 2104, https://doi.org/10.1103/PhysRevC.50.2104.
[3] H. Esbensen, G.F. Bertsch, Nucl. Phys. A 600 (1996) 37, https://doi.org/10.1016/0375-9474(96)00006-1.
[4] T. Kido, K. Yabana, Y. Suzuki, Phys. Rev. C 50 (1994) R1276–R1279, https://doi.org/10.1103/PhysRevC.50.R1276.
[5] P. Capel, G. Goldstein, D. Baye, Phys. Rev. C 70 (2004) 064605, https://doi.org/10.1103/PhysRevC.70.064605.
[6] A. Deltuva, A.M. Moro, E. Cravo, F.M. Nunes, A.C. Fonseca, Phys. Rev. C 76 (2007) 064602, https://doi.org/10.1103/PhysRevC.76.064602.
[7] N.C. Summers, F.M. Nunes, I.J. Thompson, Phys. Rev. C 74 (2006) 014606, https://doi.org/10.1103/PhysRevC.74.014606.
[8] R. de Diego, J.M. Arias, J.A. Lay, A.M. Moro, Phys. Rev. C 89 (6) (2014) 064609, https://doi.org/10.1103/PhysRevC.89.064609.
[9] R. de Diego, R. Crespo, A.M. Moro, Phys. Rev. C 95 (2017) 044611, https://doi.org/10.1103/PhysRevC.95.044611.
[10] J.A. Lay, R. de Diego, R. Crespo, A.M. Moro, J.M. Arias, R.C. Johnson, Phys. Rev. C 94 (2016) 021602, https://doi.org/10.1103/PhysRevC.94.021602.
[11] G. Baur, R. Shyam, F. Rosel, D. Trautmann, Phys. Rev. C 21 (1980) 2668.
[12] T. Udagawa, T. Tamura, Phys. Rev. C 24 (1981) 1348–1349, https://doi.org/10.1103/PhysRevC.24.1348.
[13] T. Udagawa, X.H. Li, T. Tamura, Phys. Lett. B 135 (1984) 333.
[14] M. Ichimura, N. Austern, C.M. Vincent, Phys. Rev. C 32 (1985) 431, https://doi.org/10.1103/PhysRevC.32.431.
[15] M. Hussein, K. McVoy, Nucl. Phys. A 445 (1) (1985) 124–139.
[16] J. Lei, A.M. Moro, Phys. Rev. C 92 (2015) 044616, https://doi.org/10.1103/PhysRevC.92.044616.
[17] G. Potel, F.M. Nunes, I.J. Thompson, Phys. Rev. C 92 (2015) 034611, https://doi.org/10.1103/PhysRevC.92.034611.
[18] B. Carlson, R. Capote, M. Sin, Few-Body Syst. 57 (5) (2016) 307–314, https://doi.org/10.1007/s00601-016-1054-8.
[19] A. Di Pietro, et al., Phys. Rev. Lett. 105 (2010) 022701, https://doi.org/10.1103/PhysRevLett.105.022701.
[20] A. Di Pietro, et al., Phys. Rev. C 85 (2012) 054607, https://doi.org/10.1103/PhysRevC.85.054607.
[21] N. Keeley, N. Alamanos, K.W. Kemper, K. Rusek, Phys. Rev. C 82 (2010) 034606, https://doi.org/10.1103/PHYSREVC.82.034606.
[22] T. Druet, P. Descouvemont, Eur. Phys. J. A 48 (2012) 147, https://doi.org/10.1140/epja/i2012-12147-9.
[23] W.Y. So, K.S. Kim, K.S. Choi, M.-K. Cheoun, Phys. Rev. C 92 (2015) 014627, https://doi.org/10.1103/PhysRevC.92.014627.
[24] W.Y. So, K.S. Choi, M.-K. Cheoun, K.S. Kim, Phys. Rev. C 93 (2016) 054624, https://doi.org/10.1103/PhysRevC.93.054624.
[25] D. Torresi, et al., Nucl. Instrum. Methods Phys. Res., Sect. A, Accel. Spectrom. Detect. Assoc. Equip. 713 (2013) 11–18, https://doi.org/10.1016/j.nima.2013.02.027.
[26] L. Grassi, et al., Nucl. Instrum. Methods Phys. Res., Sect. A, Accel. Spectrom. Detect. Assoc. Equip. 767 (2014) 99–111, https://doi.org/10.1016/j.nima.2014.08.009.
[27] T. Tarutina, L.C. Chamon, M.S. Hussein, Phys. Rev. C 67 (2003) 044605, https://doi.org/10.1103/PhysRevC.67.044605.
[28] F.M. Nunes, J.A. Christley, I.J. Thompson, R.C. Johnson, V.D. Efros, Nucl. Phys. A 609 (1996) 43, https://doi.org/10.1016/0375-9474(96)00284-9.
[29] A. Calci, P. Navrátil, R. Roth, J. Dohet-Eraly, S. Quaglioni, G. Hupin, Phys. Rev. Lett. 117 (2016) 242501, https://doi.org/10.1103/PhysRevLett.117.242501.
[30] B. Morillon, P. Romain, Phys. Rev. C 70 (2004) 014601, https://doi.org/10.1103/PhysRevC.70.014601.
[31] V. Pesudo, et al., Phys. Rev. Lett. 118 (2017) 152502, https://doi.org/10.1103/PhysRevLett.118.152502.
[32] D.J. Millener, J.W. Olness, E.K. Warburton, S.S. Hanna, Phys. Rev. C 28 (1983) 497, https://doi.org/10.1103/PhysRevC.28.497.
[33] J.A. Tostevin, F.M. Nunes, I.J. Thompson, Phys. Rev. C 63 (2001) 024617, https://doi.org/10.1103/PhysRevC.63.024617.
[34] A.M. Moro, R. Crespo, Phys. Rev. C 85 (2012) 054613, https://doi.org/10.1103/PhysRevC.85.054613.
[35] A.M. Moro, R. de Diego, J.A. Lay, R. Crespo, R.C. Johnson, J.M. Arias, J. Gómez-Camacho, in: AIP Conference Proceedings-American Institute of Physics, vol. 1491, 2012, p. 335.